ELSEVIER

Journal of Fluids and Structures 26 (2010) 1058–1077

JOURNAL OF FLUIDS AND STRUCTURES

www.elsevier.com/locate/jfs

Nonlinear simulation of a tuned liquid damper with damping screens using a modal expansion technique

J.S. Love, M.J. Tait*

Department of Civil Engineering, McMaster University, 1280 Main St. W., Hamilton, Ont., Canada L8S 4L7

Received 6 October 2009; accepted 20 July 2010
Available online 23 October 2010

Abstract

Tuned liquid dampers utilize sloshing fluid to control wind-induced structural motions. However, as a result of the nonlinear free surface boundary conditions of fluid sloshing in a two-dimensional rectangular container, a closed-form solution describing the response behaviour is unavailable. Modal expansions, which couple the sloshing modes, are carried out to the first, third and fifth order to construct a system of coupled nonlinear ordinary differential equations that are solved using the Runge–Kutta–Gill Method. Modal damping is incorporated to account for energy losses arising from the fluid viscosity and the inclusion of damping screens. The model is in general agreement with a previous third-order model that incorporated screen damping in the fundamental sloshing mode only. Sinusoidal shake table experiments are conducted to validate the proposed models. Response time histories and frequency response plots assess the model's prediction of wave heights, sloshing forces, and screen forces. The first-order model accurately predicts the resonant sloshing forces, and forces on a mid-tank screen. The higher-order models better represent the wave heights and forces on an off-centre screen. Experimental results from structure–TLD system tests under random excitation are used to evaluate the performance of the proposed models. The first-order model is able to predict the variance of the structural response and the effective damping the TLD adds to the structure, but as a minimum, a third-order model should be employed to predict the fluid response. It is concluded that a first-order model can be utilized for preliminary TLD design, while a higher-order model should be used to determine the required tank freeboard and the loading on damping screens positioned at off-centre locations.

Keywords: Tuned liquid damper; Modal expansion; Damping screens; System tests; Nonlinear sloshing

1. Introduction

Building trends have led to taller, lighter, more flexible and lightly damped structures. Structures having these characteristics are more susceptible to wind-induced dynamic motion. A number of devices have been developed to reduce this motion, one of the simplest being the tuned liquid damper (Kareem et al., 1999). A tuned liquid damper (TLD) consists of a tank, partially filled with a liquid (usually water), which is typically located near the top of a structure. When the tank is excited through structural motion, the fluid in the TLD tank begins to slosh, imparting inertial forces onto the structure, out of phase with the structural motion, thereby reducing the movement.

*Corresponding author. Tel.: +1 905 525 9140x26469; fax: +1 905 529 9688.
E-mail address: taitm@mcmaster.ca (M.J. Tait).

0889-9746/$ - see front matter © 2010 Elsevier Ltd. All rights reserved.
doi:10.1016/j.jfluidstructs.2010.07.004

Equivalently, one can view the effect of the device as transferring vibrational energy from the structure to the sloshing fluid where it is dissipated through damping mechanisms in the tank. An optimal damping ratio exists that results in optimal performance of the TLD (Warburton, 1982), however the inherent liquid viscous damping is usually significantly less than this quantity. Screens, poles, baffles and other flow restricting devices are often inserted into the tank to achieve the optimal damping ratio (Tait et al., 2005).

Although the simplicity of its construction and maintenance makes a TLD cost effective, its nonlinear behaviour makes modelling and designing these devices challenging. Potential flow theory is often used to determine the sloshing response of the liquid in the tank. While the governing equation of potential flow theory is linear, the free-surface boundary conditions are nonlinear and no closed-form solution is known (Le Mehaute, 1976). In addition, the damping arising from the insertion of slat-type damping screens is proportional to the square of the fluid velocity, making the damping ratio of a TLD dependent on the amplitude of sloshing (Tait, 2008).

Numerous methods have been employed to solve the problem of sloshing water in a rectangular container. The most basic is to linearize the free-surface boundary conditions by neglecting the nonlinear terms. Although this makes the solution quite straightforward, it is only valid for small fluid response amplitudes. However, for larger fluid response amplitudes, where the nonlinear terms cannot be neglected, a modal expansion can be carried out in which the modes are coupled through the nonlinear free surface boundary conditions (Kaneko and Yoshida, 1999; Faltinsen et al., 2000). As more sloshing modes are included in the modal expansion, that is, as the order of the model increases, the accuracy is improved. Hereafter, first-, third- and fifth-order models refer to models which consider one (linearized model), three and five modes, respectively.

A brief overview of the expansion method is presented, but reference is made to the work of Faltinsen et al. (2000) for detailed derivations. The expansion technique is extended to allow the incorporation of modal damping arising from the viscous fluid and insertion of slat-type damping screens. The Runge–Kutta–Gill Method is utilized to solve the system of nonlinear ordinary differential equations developed by the expansion. This model is compared to a third-order model developed by Kaneko and Yoshida (1999), which incorporated fundamental mode damping due to fluid drag on a submerged net. The present method permits the addition of energy dissipation, resulting from the implementation of flow restricting devices, to all modes considered.

The numerical outputs are compared to experimental results obtained from shake table experiments to validate the model over a range of tank sizes, damping screen configurations, and excitation frequencies. The TLD response quantities of interest in this study are wave heights, sloshing forces and the forces exerted on the damping screens. Time histories of the modelled and experimental results are presented which demonstrate the capabilities and limitations of each model order. Frequency response plots are created which show the maximum and minimum wave heights, the maximum sloshing forces and the maximum screen forces over a set of discrete excitation frequencies in the vicinity of the fundamental sloshing frequency. Lastly, the models are coupled with a linear structure, allowing the response of a structure–TLD system to be predicted. They are then validated with structure–TLD system tests where the structure is subjected to random force excitation. With these comparisons it is possible to establish which TLD response quantities can be represented with sufficient accuracy through a linearized model, and which response quantities require a higher-order model.

2. Modal expansion

Modal expansion techniques of Faltinsen et al. (2000) and Faltinsen and Timokha (2001) are utilized in this paper. The fluid flow is assumed to be inviscid, irrotational and incompressible. The two dimensional coordinate system for the tank is seen in Fig. 1. For a rectangular tank, the (disturbance) velocity potential, ϕ and the free surface, η are expressed as an infinite summation of sloshing modes:

$$\phi(x,z,t)=\sum_{m=1}^{\infty} R_m(t)\cos\left(\frac{m\pi}{L}x\right)\frac{\cosh(m\pi(z+h)/L)}{\cosh(m\pi h/L)}, \tag{1}$$

$$\eta(x,t)=\sum_{m=1}^{\infty} \beta_m(t)\cos\left(\frac{m\pi}{L}x\right), \tag{2}$$

where $R_m(t)$ and $\beta_m(t)$ are the time dependent generalized coordinates of the mth sloshing mode, h is the still water fluid depth and L is the length of the tank. The infinite summations of Eqs. (1) and (2) must be truncated at some point, which establishes the order of the solution.

Faltinsen et al. (2000) present derivations to solve the nonlinear sloshing in a tank undergoing up to six types of excitation (rotation about three axes and translation along three axes); however, only translation along the x-axis is

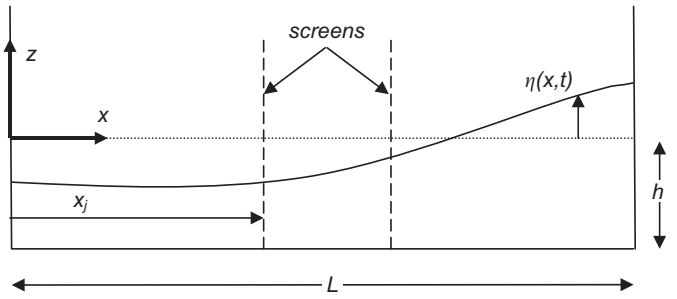

Fig. 1. Coordinate system of tank.

considered in this study. The development of the system of differential equations is based on the Bateman–Luke variational principle (Bateman, 1944; Luke, 1967), in which the pressure function, $p-p_0$ is minimized through the fluid volume

$$L=-\rho\int_{Q(t)}(p-p_0)\,dQ=-\rho\int_{Q(t)}\left(\frac{\partial\Phi}{\partial t}+\frac{1}{2}(\nabla\Phi)^2-\nabla\Phi\dot{X}-gz\right)dQ, \tag{3}$$

where $Q(t)$ is the time-dependent volume of the fluid, ρ is the density, g is the acceleration due to gravity, X is the displacement of the tank in the x-direction and an overdot denotes a time derivative. Here the total velocity potential, Φ is defined as

$$\Phi(x,z,t)=\dot{X}x+\phi(x,z,t). \tag{4}$$

The boundary conditions of the sloshing problem can be found explicitly by applying calculus of variations to the functional given by (Luke, 1967; Hargreaves, 1908)

$$W=\int_{t_1}^{t_2}L\,dt. \tag{5}$$

Faltinsen et al. (2000) apply calculus of variations to Eq. (5) to develop two equations: one through the variation of the free surface, $\delta\beta_m(t)$, and the other through the variation of the velocity potential, $\delta R_m(t)$. These two equations are used with the modal expansions of Eqs. (1) and (2) to develop a system of coupled ordinary differential equations as functions of $\beta_m(t)$. Faltinsen et al. (2000) present a sample third-order solution for a two-dimensional (2-D) rectangular tank. In Faltinsen and Timokha (2001) the method is used to develop a fifth-order solution to the same problem.

As higher sloshing modes are considered, the magnitude of their contributions to the overall response decreases; therefore, it is assumed that certain higher-order interactions can be neglected. This is equivalent to neglecting terms that result in higher powers of a small expansion parameter, ε (Waterhouse, 1994; Tadjbakhsh and Keller, 1960). In this study, an interaction term is only considered if the sum of the interacting modes is equal to or less than the model order. The omission of higher-order interaction terms was seen to have a negligible impact on the simulations.

2.1. Incorporation of modal damping

The simultaneous ordinary differential equations of Faltinsen et al. (2000) and Faltinsen and Timokha (2001) do not contain terms to account for damping. Faltinsen et al. (2005) estimated damping arising from viscous effects, but damping from flow restricting devices was not considered. In this paper, additional terms are introduced to accommodate energy dissipation arising from fluid viscosity and the inclusion of damping screens.

Miles (1967) has shown the viscosity of fluid sloshing in a rectangular container produces a damping ratio for the mth mode equal to

$$\zeta_{w,m}=\left(\frac{1}{L}\right)\sqrt{\frac{\upsilon}{2\omega_m}}\left(\frac{L}{b}+1+m\pi\left[1-2\frac{h}{L}\right]\operatorname{cosech}\left(2\frac{m\pi}{L}h\right)+m\pi\coth\left(\frac{m\pi}{L}h\right)\right), \tag{6}$$

where υ is the fluid viscosity, b is the tank width and ω_m is the natural angular frequency of the mth sloshing mode, defined as

$$\omega_m^2 = \frac{m\pi g}{L}\tanh\left(\frac{m\pi h}{L}\right). \tag{7}$$

Tait (2008) used the principle of virtual work to calculate the modal damping ratio produced by a screen based on linear sloshing theory. The damping due to the screens can be related to the magnitude of the fluid response

$$\zeta_{s,m} = \frac{\tanh(m\pi h/L)}{2\omega_m L} C_l \left(\frac{1}{3} + \frac{1}{\sinh^2(m\pi h/L)}\right) \sum_{j=1}^{ns} \left|\sin^3\left(\frac{m\pi x_j}{L}\right)\right| |\dot{\beta}_m(t)|, \tag{8}$$

where ns is the number of screens and x_j is the location of the jth screen. These modal damping terms are incorporated into the set of nonlinear differential equations.

2.2. System of nonlinear ordinary differential equations

The system of equations for the third-order expansion is

$$\begin{aligned}
&\ddot{\beta}_m + 2\omega_m(\zeta_{w,m}+\zeta_{s,m})\dot{\beta}_m + \omega_m^2\beta_m + P_m\ddot{X} + \ddot{\beta}_1[\beta_2 D_1^m(1,2) + \beta_1 D_1^m(1,1)] + \ddot{\beta}_2[\beta_1 D_1^m(2,1)] + \ddot{\beta}_1[\beta_1\beta_1 D_2^m(1,1,1)] \\
&\quad + \dot{\beta}_1[\dot{\beta}_1 T_0^m(1,1)] + \dot{\beta}_2[\dot{\beta}_1 T_0^m(2,1)] + \dot{\beta}_1^2[\beta_1 T_1^m(1,1,1)] = 0,
\end{aligned} \tag{9}$$

where the constants, D_i, T_i and P_i (Appendix A) are derived by Faltinsen and Timokha (2001), and the superscript or subscript m refers to the sloshing mode being considered. Similarly, the system of equations for the fifth-order expansion is

$$\begin{aligned}
&\ddot{\beta}_m + 2\omega_m[\zeta_{w,m}+\zeta_{s,m}]\dot{\beta}_m + \omega_m^2\beta_m + P_m\ddot{X} + \ddot{\beta}_1[\beta_4 D_1^m(1,4) + \beta_3 D_1^m(1,3) + \beta_2 D_1^m(1,2) + \beta_1 D_1^m(1,1)] \\
&\quad + \ddot{\beta}_2[\beta_3 D_1^m(2,3) + \beta_2 D_1^m(2,2) + \beta_1 D_1^m(2,1)] + \ddot{\beta}_3[\beta_2 D_1^m(3,2) + \beta_1 D_1^m(3,1)] + \ddot{\beta}_4[\beta_1 D_1^m(4,1)] \\
&\quad + \ddot{\beta}_1[\beta_3\beta_1 D_2^m(1,3,1) + \beta_2\beta_2 D_2^m(1,2,2) + \beta_2\beta_1 D_2^m(1,2,1) + \beta_1\beta_1 D_2^m(1,1,1)] \\
&\quad + \ddot{\beta}_2[\beta_2\beta_1 D_2^m(2,2,1) + \beta_1\beta_1 D_2^m(2,1,1)] + \ddot{\beta}_3[\beta_1\beta_1 D_2^m(3,1,1)] \\
&\quad + \ddot{\beta}_1[\beta_2\beta_1\beta_1 D_3^m(1,2,1,1) + \beta_1\beta_1\beta_1 D_3^m(1,1,1,1)] + \ddot{\beta}_2[\beta_1\beta_1\beta_1 D_3^m(2,1,1,1)] + \ddot{\beta}_1[\beta_1\beta_1\beta_1\beta_1 D_4^m(1,1,1,1,1)] \\
&\quad + \dot{\beta}_1[\dot{\beta}_1 T_0^m(1,1)] + \dot{\beta}_2[\dot{\beta}_2 T_0^m(2,2) + \dot{\beta}_1 T_0^m(2,1)] + \dot{\beta}_3[\dot{\beta}_2 T_0^m(3,2) + \dot{\beta}_1 T_0^m(3,1)] + \dot{\beta}_4[\dot{\beta}_1 T_0^m(4,1)] \\
&\quad + \dot{\beta}_1\dot{\beta}_1[\beta_3 T_1^m(1,1,3) + \beta_2 T_1^m(1,1,2) + \beta_1 T_1^m(1,1,1)] \\
&\quad + \dot{\beta}_2\dot{\beta}_2[\beta_1 T_1^m(2,2,1)] + \dot{\beta}_2\dot{\beta}_1[\beta_2 T_1^m(2,1,2) + \beta_1 T_1^m(2,1,1)] + \dot{\beta}_3\dot{\beta}_1[\beta_1 T_1^m(3,1,1)] \\
&\quad + \dot{\beta}_1\dot{\beta}_1[\beta_2\beta_1 T_2^m(1,1,2,1) + \beta_1\beta_1 T_2^m(1,1,1,1)] + \dot{\beta}_2\dot{\beta}_1[\beta_1\beta_1 T_2^m(2,1,1,1)] + \dot{\beta}_1\dot{\beta}_1[\beta_1\beta_1\beta_1 T_3^m(1,1,1,1,1)] = 0.
\end{aligned} \tag{10}$$

The simultaneous ordinary differential equations are solved using the Runge–Kutta–Gill Method.

With the generalized coordinates of the free surface determined, it is possible to solve for the generalized coordinates of the velocity potential, $R_m(t)$. For the third-order model, Faltinsen and Timokha (2001) have shown that $R_m(t)$ can be expressed as

$$R_m = \frac{\dot{\beta}_m}{2E_m} + \sum_{i=1}^{3}\sum_{j=1}^{3} \dot{\beta}_i\beta_j V_{i,j}^{2,m} + \sum_{i=1}^{3}\sum_{j=1}^{3}\sum_{p=1}^{3} \dot{\beta}_i\beta_j\beta_p V_{i,j,p}^{3,m}, \tag{11}$$

where the constants V_i are defined in Appendix A. Similarly, for the fifth-order expansion,

$$\begin{aligned}
R_m = &\frac{\dot{\beta}_m}{2E_m} + \sum_{i=1}^{5}\sum_{j=1}^{5} \dot{\beta}_i\beta_j V_{i,j}^{2,m} + \sum_{i=1}^{5}\sum_{j=1}^{5}\sum_{p=1}^{5} \dot{\beta}_i\beta_j\beta_p V_{i,j,p}^{3,m} + \sum_{i=1}^{5}\sum_{j=1}^{5}\sum_{p=1}^{5}\sum_{q=1}^{5} \dot{\beta}_i\beta_j\beta_p\beta_q V_{i,j,p,q}^{4,m} \\
&+ \sum_{i=1}^{5}\sum_{j=1}^{5}\sum_{p=1}^{5}\sum_{q=1}^{5}\sum_{r=1}^{5} \dot{\beta}_i\beta_j\beta_p\beta_q\beta_r V_{i,j,p,q,r}^{5,m}.
\end{aligned} \tag{12}$$

To reduce the size of Eqs. (11) and (12) with negligible loss of accuracy, terms in which the indices of the βs sum to more than the model order are neglected.

Both Eqs. (11) and (12) can be differentiated with respect to time to find the first derivative of the velocity potential generalized coordinate, $\dot{R}_m(t)$, which is required to calculate the acceleration of fluid particles. For the third-order model,

$$\dot{R}_m = \frac{\ddot{\beta}_m}{2E_m} + \sum_{i=1}^{3}\sum_{j=1}^{3} \ddot{\beta}_i\beta_j \left(V_{i,j}^{2,m} + \sum_{p=1}^{3} \beta_p V_{i,j,p}^{3,m} \right) + \sum_{i=1}^{3}\sum_{j=1}^{3} \dot{\beta}_i\dot{\beta}_j \left(V_{i,j}^{2,m} + 2\sum_{p=1}^{3} \beta_p \overline{V}_{i,j,p}^{3,m} \right), \tag{13}$$

where constants $\overline{V}$ are found in Appendix A. For the fifth-order model,

$$\begin{aligned}\dot{R}_m = {} & \frac{\ddot{\beta}_m}{2E_m} + \sum_{i=1}^{5}\sum_{j=1}^{5} \ddot{\beta}_i\beta_j \left(V_{i,j}^{2,m} + \sum_{p=1}^{5} \beta_p V_{i,j,p}^{3,m} + \sum_{p=1}^{5}\sum_{q=1}^{5} \beta_p\beta_q V_{i,j,p,q}^{4,m} + \sum_{p=1}^{5}\sum_{q=1}^{5}\sum_{r=1}^{5} \beta_p\beta_q\beta_r V_{i,j,p,q,r}^{5,m} \right) \\ & + \sum_{i=1}^{5}\sum_{j=1}^{5} \dot{\beta}_i\dot{\beta}_j \left(V_{i,j}^{2,m} + 2\sum_{p=1}^{5} \beta_p \overline{V}_{i,j,p}^{3,m} + 3\sum_{p=1}^{5}\sum_{q=1}^{5} \beta_p\beta_q \overline{V}_{i,j,p,q}^{4,m} + 4\sum_{p=1}^{5}\sum_{q=1}^{5}\sum_{r=1}^{5} \beta_p\beta_q\beta_r \overline{V}_{i,j,p,q,r}^{4,m} \right).\end{aligned} \tag{14}$$

With the two time-dependent variables, β_m and R_m known, Eq. (2) can be used to determine the wave height at any location along the length of the tank and the gradient of Eq. (1) can be used to find the velocity of the fluid.

3. Determination of TLD response quantities

3.1. Wave heights

For any specified x-coordinate in the tank, the wave height of the fluid can be determined by Eq. (2). The wave heights are of particular importance at the tank end walls and at the location of screens. At the walls, the maximum wave height is used to determine the required freeboard to avoid overtopping or wave impact with the tank lid. At the screen locations, the wave height is required for calculations to determine the forces exerted on the screens by the fluid.

3.2. Sloshing forces

The sloshing forces are determined by tracking the centre of mass (centroid) of the sloshing fluid. Faltinsen and Timokha (2001) have shown that the centre of mass of the sloshing fluid is given by

$$x_C = -\frac{L}{\pi^2 h}\sum_{m=1}^{\infty} \beta_m(t)\frac{1}{m^2}\left[1+(-1)^{m+1}\right]. \tag{15}$$

Since $\beta_m(t)$ is the only time-dependent function in Eq. (15), it can be differentiated with respect to time twice to determine the acceleration of the centre of mass of the sloshing fluid. The sloshing force is calculated by multiplying the acceleration of the fluid's centre of mass by the fluid mass

$$F_{sw} = -m_w\frac{L}{\pi^2 h}\sum_{m=1}^{\infty} \ddot{\beta}_m(t)\frac{1}{m^2}\left[1+(-1)^{m+1}\right], \tag{16}$$

where m_w is the mass of the fluid, calculated as

$$m_w = \rho b h L. \tag{17}$$

There is a conservative inertial component associated with the fluid as if it were moving as a rigid mass with the tank. Therefore, the base shear force exerted by the TLD is

$$F_{TLD} = -m_w\left\{ \ddot{X} + \frac{L}{\pi^2 h}\sum_{m=1}^{\infty} \ddot{\beta}_m(t)\frac{1}{m^2}\left[1+(-1)^{m+1}\right] \right\}. \tag{18}$$

3.3. Screen forces

The purpose of screens is to increase the energy dissipation of the fluid; however, the forces on the screens must be known to ensure they are designed to have adequate structural strength.

The force exerted on an object by an accelerating fluid has an inertial and a drag component (Morison et al., 1950):

$$dF(x,z,t) = dF_d(x,z,t) + dF_i(x,z,t). \tag{19}$$

The drag forces are proportional to the velocity of the fluid squared,

$$dF_d(x_j,z,t) = \frac{1}{2}\rho C_l \frac{\partial\phi}{\partial x}\left|\frac{\partial\phi}{\partial x}\right| dA_{sc}, \tag{20}$$

where x_j is the x-coordinate of the screen location, dA_{sc} is an infinitesimal area of the screen and C_l is the screen loss coefficient, which for a slat screen can be found through empirical relationships (Tait et al., 2005) or experimentally.

The inertial forces are proportional to the acceleration of the fluid particles around the screen:

$$dF_i(x_j,z,t) = \rho t_b S C_m \left(\frac{\partial^2\phi}{\partial x\partial t}\right) dA_{sc}, \tag{21}$$

where C_m is the coefficient of mass which is determined empirically, t_b is the thickness of the slat screen and S is the screen solidity defined as the ratio of the area of the submerged slats to the total area of the submerged screen.

To determine the total force on the screen, Eq. (19) is integrated over the screen area,

$$F_{scrn}(x_j,t) = \frac{1}{2}\rho b C_l \int_{-h}^{\eta(x_j,t)} \frac{\partial\phi}{\partial x}\left|\frac{\partial\phi}{\partial x}\right| dz + \rho b S t_b C_m \int_{-h}^{\eta(x_j,t)} \left(\frac{\partial^2\phi}{\partial x\partial t}\right) dz + m_{sc}\ddot{X}, \tag{22}$$

where the integrations ranging from the bottom of the tank, $-h$ to the wave height at the screen location, $\eta(x_j,t)$ are:

$$\int_{-h}^{\eta(x_j,t)} \left(\frac{\partial^2\phi}{\partial x\partial t}\right) dz = -\sum_{m=1}^{N} \dot{R}_m \sin\left(\frac{m\pi}{L}x_j\right) \frac{\sinh(m\pi[\eta(x_j,t)+h]/L)}{\cosh(m\pi h/L)}, \tag{23}$$

$$\int_{-h}^{\eta(x_j,t)} \frac{\partial\phi}{\partial x}\left|\frac{\partial\phi}{\partial x}\right| dz = -\frac{1}{L}\sum_{m=1}^{N}\sum_{n=1}^{N} |R_m| R_n G_m(x_j) G_n(x_j) \Theta_{m,n}(x_j,t), \tag{24}$$

where N is the order of the model and the functions $G_i(x)$ and $\Theta_{m,n}(x,t)$ are defined as

$$G_m(x) = m\pi \sin\left(\frac{m\pi}{L}x\right) \frac{1}{\cosh(m\pi h/L)}, \tag{25}$$

$$\Theta_{m,n}(x,t) = \frac{\sinh((m-n)\pi[h+\eta(x,t)]/L)}{2(m-n)\pi} + \frac{\sinh((m+n)\pi[h+\eta(x,t)]/L)}{2(m+n)\pi}. \tag{26}$$

When $m = n$, Eq. (26) is evaluated using the limit

$$\lim_{x\to 0} \frac{\sinh(x\pi H)}{x\pi} = H \tag{27}$$

In Eq. (22) the inertial force arising from the mass of the screen, m_{sc} is included in this study, but is often negligible in comparison to the fluid forces.

3.4. Non-dimensional quantities

The results displayed in the subsequent sections are normalized. Time is normalized by multiplying it by the excitation frequency (in Hertz), f, given by

$$f = \frac{\omega_{exc}}{2\pi}, \tag{28}$$

where ω_{exc} is the angular excitation frequency. For the shake table tests, the angular excitation frequency is normalized with respect to the fundamental sloshing frequency

$$\beta = \frac{\omega_{exc}}{\omega_1} \tag{29}$$

and the excitation amplitude, A is normalized with respect to the tank length

$$\Lambda = \frac{A}{L}. \tag{30}$$

The wave height is normalized by the mean fluid depth

$$\eta' = \frac{\eta}{h}. \tag{31}$$

The sloshing force and the screen forces are normalized with respect to the maximum inertial force of the fluid if it moved as a rigid mass

$$F'_{sw} = \frac{F_{sw}}{m_w A \omega_{exc}^2}, \quad F'_{scrn} = \frac{F_{scrn}}{m_w A \omega_{exc}^2}. \tag{32, 33}$$

4. Fluid model validation

Numerical simulations are performed to compare the present third-order model with that of Kaneko and Yoshida (1999). Subsequently, shake table experiments are conducted on rectangular tanks with different screen configurations.

4.1. Alternative expansion method

Kaneko and Yoshida (1999) conducted a modal expansion to third order which considered the damping arising from a net submerged in the fluid. A Taylor series expansion of the nonlinear free surface boundary conditions was conducted about the mean free surface ($z = 0$). Eqs. (1) and (2) were substituted into the Taylor expansion and the Galerkin method was applied to develop a system of differential equations which were functions of $R_m(t)$ and $\beta_m(t)$. These equations, which account for the coupling of the sloshing modes, were manipulated algebraically to eliminate the generalized coordinate, $R_m(t)$. The final result was a system of coupled ordinary differential equations that were functions of the free surface generalized coordinates, $\beta_m(t)$. Modal damping provided by fluid viscosity was incorporated into the model using Eq. (6). The mid-tank net was assumed to add damping only to the fundamental sloshing mode and was calculated based on a head loss through the net given by

$$\zeta_{s,1} = \frac{C_l \omega_1 L^2}{16\pi h^2 g} |\dot{\beta}_1(t)|. \tag{34}$$

The system of coupled ordinary differential equations developed are solved numerically to determine the response of the sloshing fluid.

The present model allows the incorporation of modal damping produced by damping screens for all modes considered. In addition, it readily permits the use of multiple screens located anywhere along the length of the tank. The proposed model is compared to the model developed by Kaneko and Yoshida (1999). Fig. 2 presents a frequency response plot of the normalized wave height for a rectangular tank of length $L = 1.3$ m width $b = 0.4$ m and a screen located mid-tank. Three simulations with different fluid depths, screen loss coefficients and excitation amplitudes are

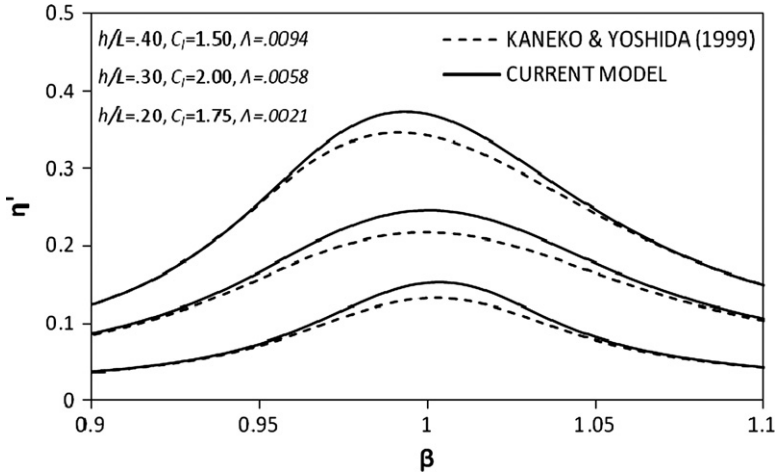

Fig. 2. Normalized wave height curves of current model and that of Kaneko and Yoshida (1999).

selected such that they produce a range of normalized fluid response amplitudes. Although both models display the same general trends, in all simulations, the proposed model predicts a greater fluid response.

4.2. Shake table experiments

Three different TLD tanks were studied experimentally having various lengths, widths, mean fluid depths, and were equipped with one, two, or three damping screens. The tanks studied were subjected to sinusoidal excitation with normalized amplitudes within the range $\Lambda = 0.005$–0.006. For each excitation amplitude, a frequency sweep of approximately 40 discrete frequencies was conducted in the vicinity of the first resonant frequency. The sloshing water was allowed to reach steady state before any recordings were taken. Table 1 displays the test identification, normalized fluid depth, screen configuration, screen loss coefficient and normalized amplitude of excitation for each test. The coefficient of mass, C_m for each screen is assumed to be 1.5, a value consistent with the findings of Tait (2004) for this type of screen.

4.3. Time history analysis

Time histories are created which describe how the fluid responds when subjected to sinusoidal base excitation. Wave heights, sloshing forces and screen forces are shown comparing the model outputs with the experimental data.

Fig. 3 shows the normalized wave height near the tank wall ($x = 0.05L$). The third- and fifth-order models are in excellent agreement with the experimental wave heights. Conversely, the first-order model only represents the first mode, which results in the underestimation of the peak heights and the overestimation of the trough depths.

Table 1
Tank configuration for shake table experiments.

Test ID	Normalized Fluid depth h/L	Screen Information		Normalized Excitation $\Lambda = A/L$
		Location(s)	C_l	
T1	0.165	$0.50L$	2.75	0.006
T2	0.182	$0.25L$, $0.50L$, $0.75L$	1.63	0.005
T3	0.123	$0.40L$, $0.60L$	2.16	0.005

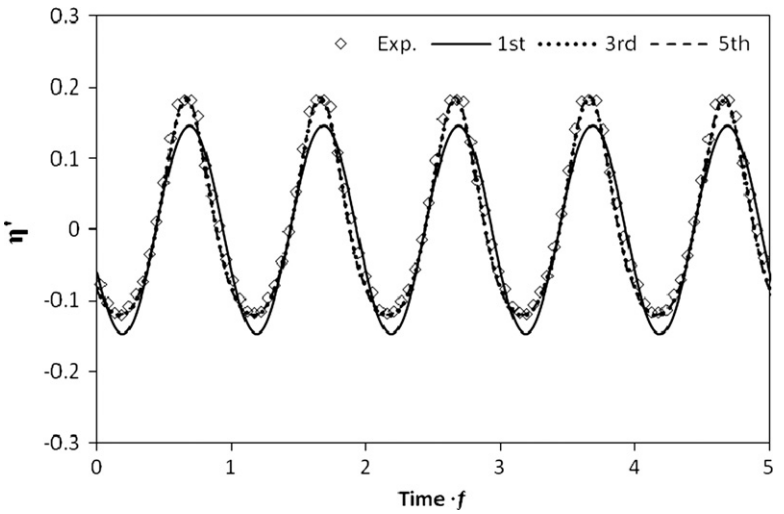

Fig. 3. Comparison of experimental and modelled normalized wave heights at tank wall for T2 ($\beta = 1.01$).

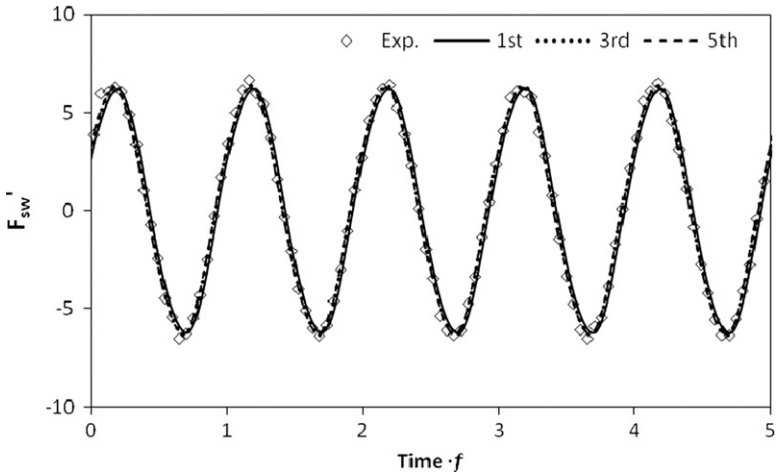

Fig. 4. Comparison of experimental and modelled normalized sloshing forces for T2 ($\beta = 1.01$).

The experimental and modelled normalized sloshing force is displayed in Fig. 4. All models are in excellent agreement with the experimental results. This agreement indicates that the most significant sloshing forces are those created by the fundamental mode.

Fig. 5 compares the experimental and modelled normalized screen forces: Fig. 5(a) represents the forces on the quarter-tank screen, located at $0.25L$, while Fig. 5(b) presents the forces on the mid-tank screen, located $0.50L$. The third- and fifth-order models are found to be in better agreement with the measured values on the quarter-tank screen as shown in Fig. 5(a). All three models accurately predict the screen forces on the mid-tank screen as shown in Fig. 5(b). At the mid-tank location, the fluid velocity is attributed mainly to the fundamental mode; therefore all models are in very good agreement.

4.4. Frequency response curves

Frequency response curves present the maximum response value for a given sinusoidal excitation frequency. Normalized frequency response curves are constructed which display: the maximum and minimum free surface elevations, the maximum sloshing forces, and the maximum screen forces. Each plot displays experimental results along with the simulated results of the first-, third- and fifth-order sloshing models.

4.4.1. Maximum and minimum wave heights

A plot showing the maximum and minimum experimental wave heights, as well as the model output is shown in Fig. 6 for T1, T2 and T3. In all tests, the first-order model is in poor agreement with the experimental data since no components of the free surface arising from higher modes is represented. The third- and fifth-order models are in good agreement with the experimental data for T2. For T1, the third-order model significantly over-predicts the free surface elevation at $\beta = 0.9$, which corresponds to the appearance of a higher harmonic in the sloshing behaviour. This excitation frequency is related to the natural frequency of the second sloshing mode by a factor of two. Since T1 has one damping screen located mid-tank, the screen does not produce any damping for the second mode, which allows a large second mode response. For T3, larger discrepancies exist between the higher-order models and the test. As will be discussed in Section 6, the excitation of higher harmonics at shallow fluid depths may cause higher sloshing modes to be overestimated (Faltinsen and Timokha, 2001).

4.4.2. Sloshing forces

Fig. 7 shows the maximum sloshing force at each excitation frequency for tests T1, T2 and T3. The models are in good to very good agreement with the experimental results. The third-order model overestimates the sloshing forces at frequency ratios values near 0.9 for T1. The first-order model does not capture the hardening behaviour of the sloshing fluid.

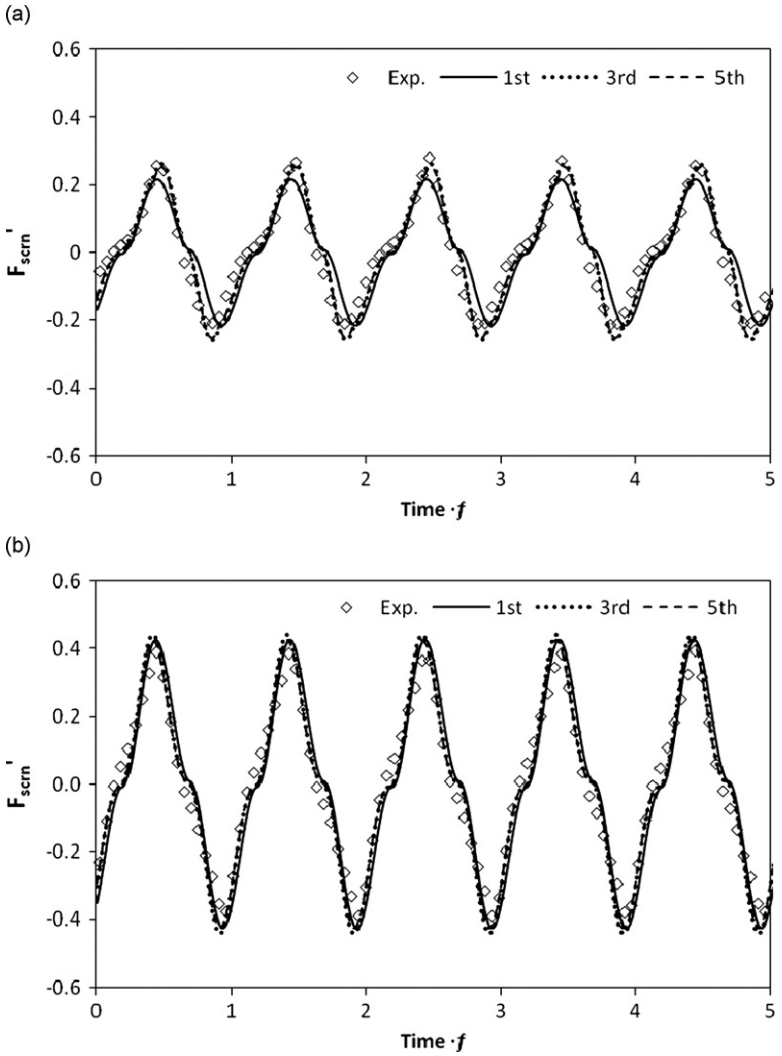

Fig. 5. Comparison of experimental and modelled screen forces for T2 ($\beta = 1.01$): (a) screen at $0.25L$ and (b) screen at $0.50L$.

4.4.3. Screen forces

Fig. 8 shows the maximum screen forces for the mid-tank and quarter-tank screens used in T2. T2 has screens at $0.25L$, $0.50L$ and $0.75L$ but measurements were only recorded for the screens at $0.25L$ and $0.50L$, since through symmetry, the screens located at the quarter-tank length experience the same forces but 180° out-of-phase. The first-order model is in poor agreement with the screen located at $0.25L$. This is expected since higher sloshing modes should have a more pronounced impact on the screen forces. The third- and fifth-order models are in good agreement with the experimental data. All models are in good agreement with the screen located at $0.50L$. The discrepancy that exists between the experimental and modelled curves is partially attributed to fluid build-up behind the screens, which was not considered by the models.

5. Structure–TLD system response

Simulations of the interaction of the structure–TLD system are validated with system tests. The linear structure is represented as a single degree of freedom system which interacts with the TLD as seen in Fig. 9(a). The system is simplified to a single degree of freedom system which is exposed to two forces; the exciting force and the force from the

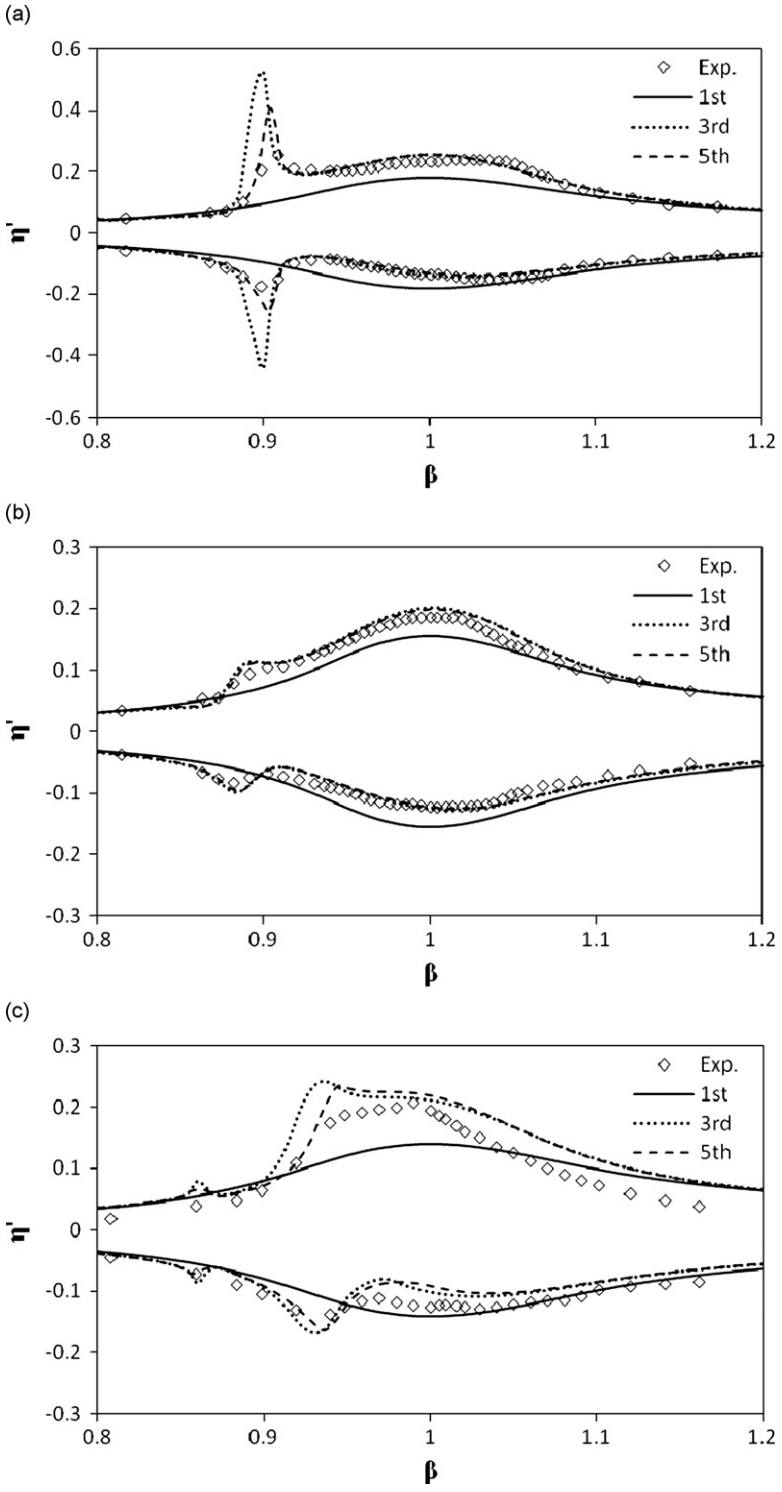

Fig. 6. Comparison of experimental and modelled frequency response curves of maximum/minimum wave height: (a) T1, (b) T2 and (c) T3.

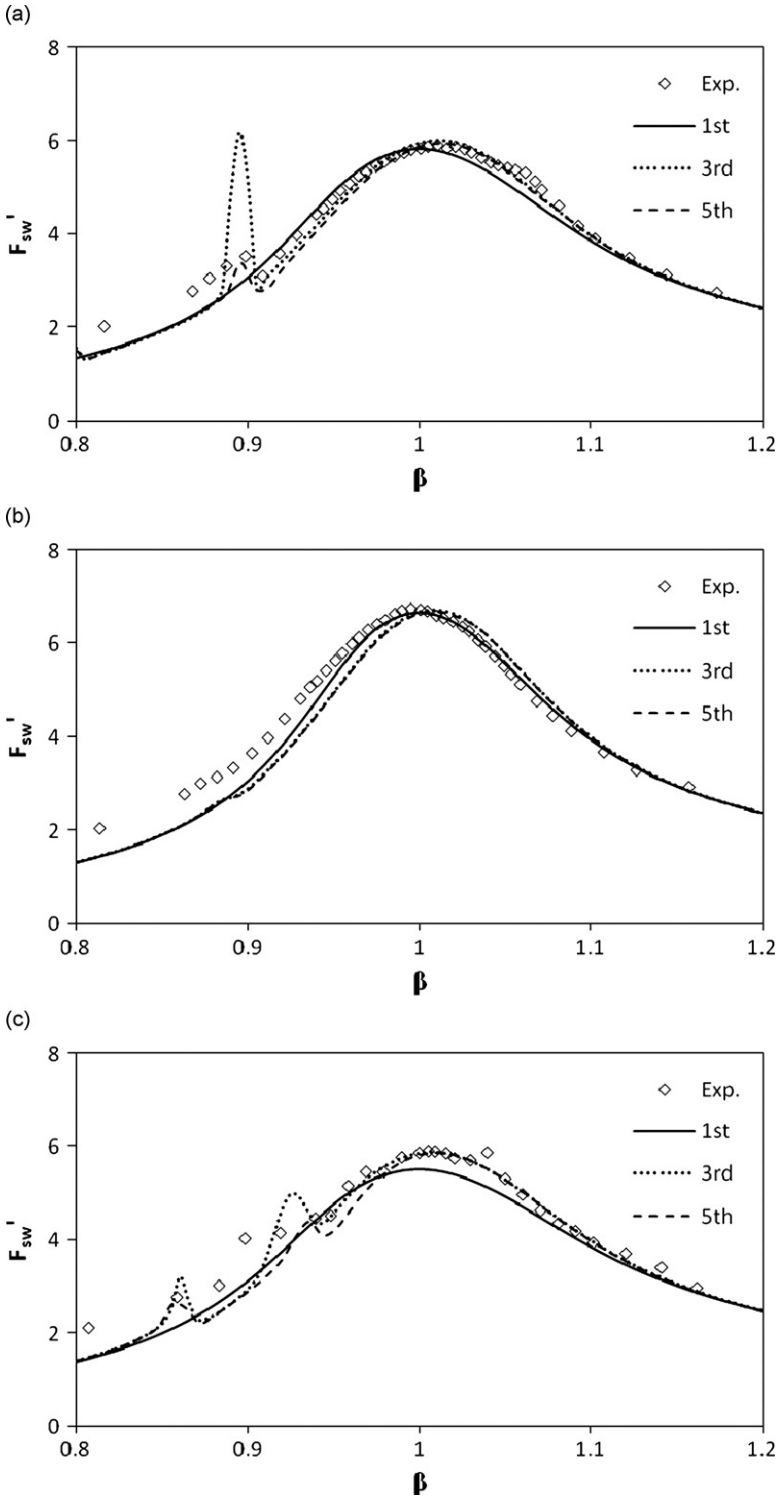

Fig. 7. Comparison of experimental and modelled maximum sloshing force versus excitation frequency: (a) T1, (b) T2 and (c) T3.

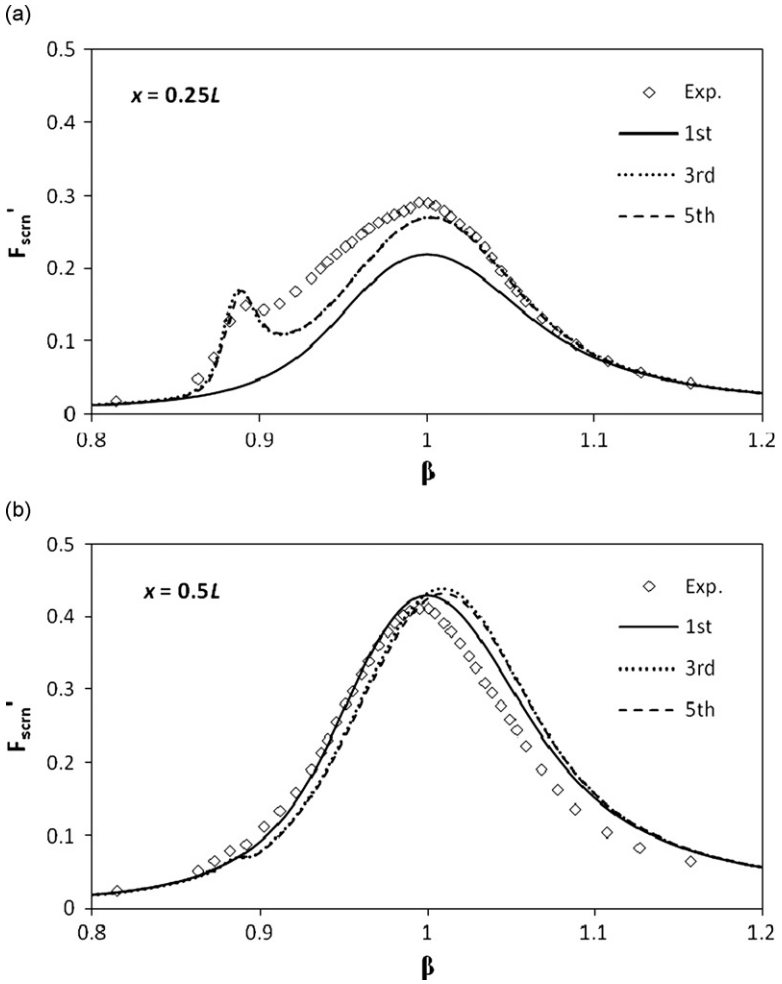

Fig. 8. Comparison of experimental and modelled maximum sloshing force versus excitation frequency for T2: (a) screen at $0.25L$ and (b) screen at $0.5L$.

TLD as shown in Fig. 9(b). Mathematically, the system can be described by the following equation of motion:

$$M\ddot{X} + C\dot{X} + KX = F_{exc} + F_{TLD}, \tag{35}$$

where M, C and K are the generalized mass, damping and stiffness of the structure, F_{exc} is the excitation force and F_{TLD} is the TLD base shear force.

Eq. (35) is a linear ordinary differential equation which can be solved numerically. The response of the structure is determined using the excitation, F_{exc}, and the TLD force, F_{TLD}, calculated using the structural acceleration $\ddot{X}$ as the excitation in Eq. (9). Eq. (18) is used to calculate the base shear force of the TLD, which is applied to the structure (along with the next excitation force) in the subsequent time step.

Structure–TLD system tests conducted by Tait (2004) are compared to the linear and third-order models. The time series and frequency response plots presented in Section 4 indicated that the fifth-order model provided negligible improvement over the third-order model, and for this reason the fifth-order model is not considered in the structure–TLD system simulations. The structure has the generalized properties: $M = 4040$ kg, $C = 14.2$ kg/s and $K = 49{,}656$ N/m. A TLD with dimensions $h = 0.119$ m, $L = 0.966$ m, $b = 0.874$ m and having damping screens located at $0.4L$ and $0.6L$ is used as an auxiliary absorber for the structure. The screen loss coefficient is $C_l = 2.16$. The primary structure is subjected to band limited white noise excitation to simulate wind loading.

The response of the structure is represented using frequency response curves which are defined according to

$$|H(f)| = \sqrt{\frac{S(f)K^2}{S_0}}, \tag{36}$$

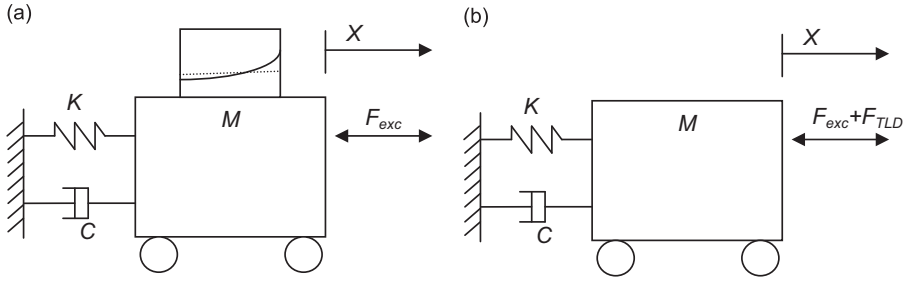

Fig. 9. Structure–TLD system representation.

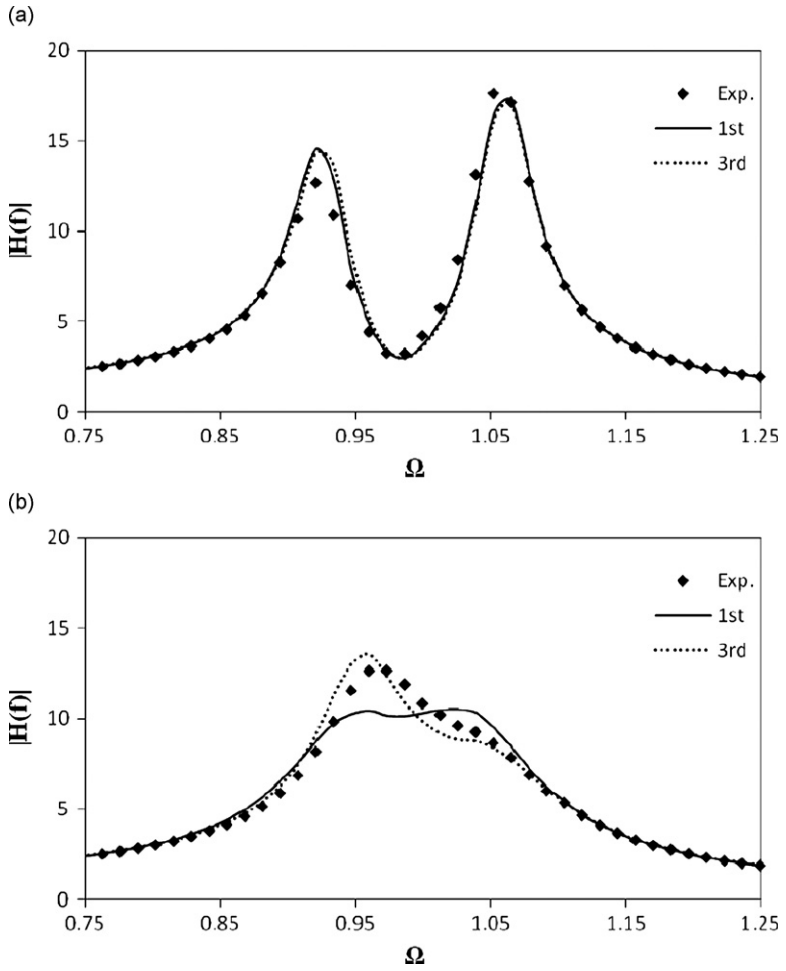

Fig. 10. Comparison of experimental and modelled frequency response for structural displacement: (a) r.m.s. force = 11.9 N and (b) r.m.s. force = 90.8 N.

where S_0 is the white noise spectrum and $S(f)$ is the response spectrum of the variable being considered. The angular natural frequency of the structure,

$$\omega_s = \sqrt{\frac{K}{M}}, \tag{37}$$

is used to normalize the excitation frequency:

$$\boldsymbol{\Omega} = \frac{\omega_{exc}}{\omega_s}. \tag{38}$$

Fig. 10 shows the structural displacement frequency response curves for root mean square (r.m.s.) excitation forces of 11.9 and 90.8 N, respectively. For the smaller excitation, both models are in very good agreement with the data. For the larger excitation, the TLD damping exceeds the optimal value, resulting in a single peaked frequency response curve. The linear model is found to underestimate the response, however the third-order model is found to be in good agreement with the data.

Fig. 11 presents frequency response curves of the liquid free surface for r.m.s. structural excitations of 11.9 and 90.8 N. Both models are in excellent agreement with the data when the r.m.s. excitation is 11.9 N. When the excitation is 90.8 N, the third-order model is found to be in better agreement with the experimental data than the first-order model.

The quantities of most interest to the structural engineer are the r.m.s. structural response and the effective damping the TLD adds to the structure (Vickery and Davenport, 1970). The r.m.s. responses of the structure, σ_s and fluid free

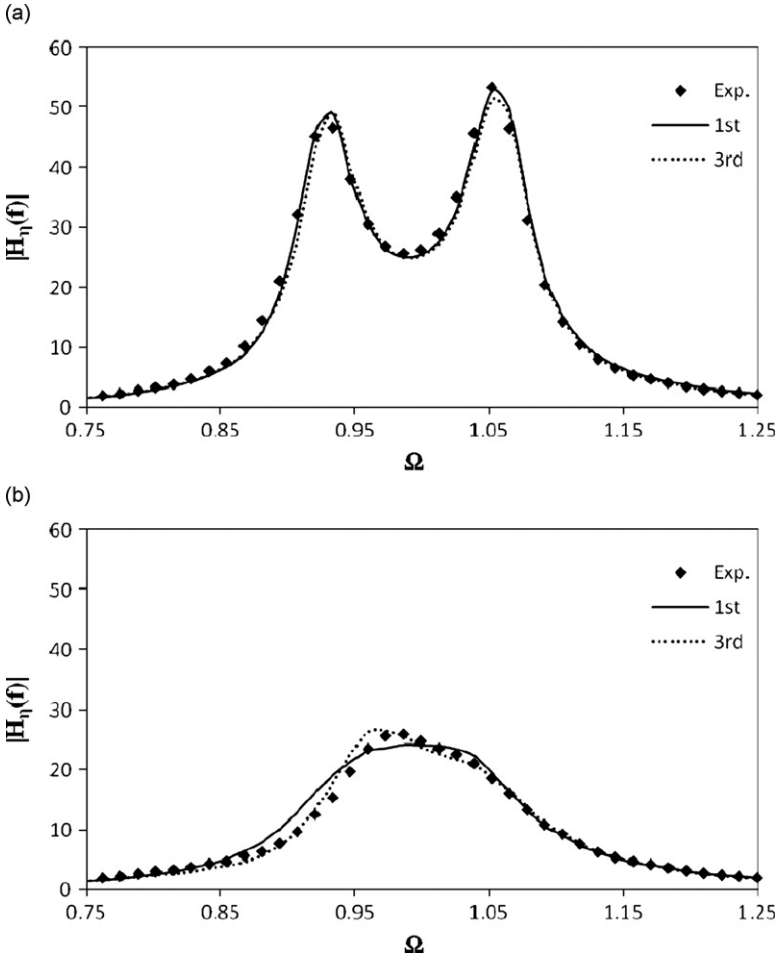

Fig. 11. Comparison of experimental and modelled frequency response for free surface amplitude (at $x = 0.05L$): (a) r.m.s. force = 11.9 N and (b) r.m.s. force = 90.8 N.

Table 2
Response of structure–TLD system under random excitation (model percent error).

Excitation		σ_s	σ_η	ζ_{eff}
r.m.s. force 11.9 N	Experiment	1.01	3.31	2.50
	1st	1.03 (2.0%)	3.22 (2.7%)	2.39 (4.4%)
	3rd	1.02 (1.0%)	3.37 (1.8%)	2.41 (3.6%)
r.m.s. force 90.8 N	Experiment	6.85	14.8	3.16
	1st	6.67 (2.6%)	13.2 (11%)	3.31 (4.7%)
	3rd	6.89 (0.5%)	15.7 (6.1%)	3.09 (2.2%)

surface, σ_η are related to the area under the frequency response curves shown in Figs. 10 and 11,

$$\sigma^2 = \frac{S_0}{K^2}\int_0^\infty |H(f)|^2\, df. \tag{39}$$

Vickery and Davenport (1970) have shown that the effective damping added to the structure by a dynamic vibration absorber is

$$\zeta_{eff} = \frac{\pi}{4} f_s \frac{1}{\int_0^\infty |H(f)\, df} - \zeta_s, \tag{40}$$

where ζ_s is the damping ratio of the structure without an absorber calculated as

$$\zeta_s = \frac{C}{2M\omega_s}. \tag{41}$$

Table 2 shows the r.m.s. structural and fluid responses (in mm) as well as the effective damping (in percentage of critical damping) for the system tested with r.m.s. force excitations of 11.9 and 90.8 N. For both excitations, the first-order model predicts the r.m.s. structural response and effective damping within 5% error of the experimental data. The error for the r.m.s. fluid response is as large as 11%. The third-order model does not display significant improvement over the linear model for the structural response and effective damping. However, the third-order model is a better representation of the variance of the fluid response with a maximum error of approximately 6%.

6. Model usage

Experimental results indicate that the wave heights and screen forces are not well represented by the first-order theory. Conversely, for small to moderate excitations, the first-order model predictions of the sloshing forces are in reasonable agreement with experimental results, particularly near resonance. The structural response is only affected by the sloshing fluid force. Therefore, the response of the structure can be established by the first-order model. The linearized model can be used to conduct a preliminary design of the tank (b, L, h), establish the required screen loss coefficient, C_l, and estimate the structural response, σ_s. The required freeboard to prevent fluid impact with the tank lid, or alternatively overtopping and fluid spillage, would require the use of a higher-order model to establish maximum wave heights. Additionally, if a screen were located away from centre, a higher-order model would be required to determine the forces to which the screens would be subjected.

The accuracy of higher-order models decreases as the mean fluid depth decreases. At small fluid depth to tank length ratios, higher harmonics are excited at frequencies close to the fundamental sloshing frequency. The excitation of higher sloshing modes can lead to the violation of the assumption that higher-order sloshing modes become increasingly insignificant. Nonlinear shallow water wave theory (Lepellitier and Raichlen, 1988; Tait et al., 2005) would be a more suitable model for small fluid depths.

7. Conclusion

The nonlinear free surface boundary conditions of fluid sloshing in a rectangular tank require that the solution utilizes approximations. The simplest approximation is to neglect the nonlinear terms in the boundary condition which

allows a relatively straightforward solution procedure that is only valid for small fluid motions. Alternatively, a modal expansion can be employed which accounts for the effects of higher sloshing modes.

Models developed by Faltinsen et al. (2000) and Faltinsen and Timokha (2001) were modified; allowing them to be used to simulate a tuned liquid damper. Energy dissipation arising from fluid viscosity, and the inclusion of damping screens in the tank was incorporated into the model. Kaneko and Yoshida (1999) employed a different modal expansion method and incorporated viscous fluid damping, as well as damping in the fundamental mode provided by a net. The model used in this paper was found to be in general agreement with Kaneko and Yoshida (1999).

The system of equations was solved using the Runge–Kutta–Gill Method, yielding the response of each sloshing mode. With the modal responses established, wave heights, sloshing forces, and damping screen forces were calculated.

Time histories and frequency response plots displayed the experimental output along with the first, third and fifth-order models under sinusoidal shake table excitation. The sloshing forces for all models were found to be in good agreement with experimental findings. Forces on a screen located mid-tank were also in good agreement for all models. The first-order (linearized) model was unable to accurately predict the wave heights and the screen forces of an off-centre screen. In addition, the linearized model was unable to capture the excitation of higher harmonics or account for the frequency shift arising from the hardening sloshing system. However, the third- and fifth-order models were in good agreement with the wave heights and screen forces. The higher-order theory shows greater discrepancies with the experimental data as the water depth decreases. For very shallow water, nonlinear shallow water wave theory may be more applicable.

The effect of a TLD on the structural response can be calculated with suitable accuracy using a linearized model. The r.m.s. structural response and the effective damping provided by the TLD were represented well by the first-order model. To determine the required freeboard, a higher-order model should be used to determine the maximum wave heights. Similarly, a higher-order model should be utilized to determine the forces to which the screens are subjected. A preliminary TLD design can be carried out using a first-order model which will allow the designer to establish the tank dimensions, the required screen loss coefficients, and the impact of the device on the structure. The individual components of the TLD, including freeboard and screen forces, should be designed using results obtained from a higher-order theory.

Acknowledgements

The authors are thankful for the financial support provided by the Natural Sciences and Engineering Research Council of Canada (NSERC) and McMaster University's Centre for Effective Design of Structures (CEDS) funded through the Ontario Research and Development Challenge Fund (ORDCF).

Appendix A. Ordinary differential equation constants

$$E_n = \frac{n\pi}{2L}\tanh\left(\frac{n\pi}{L}h\right), \quad P_{2i-1} = -\frac{8E_{2i-1}L}{\pi^2(2i-1)^2}, \quad P_{2i} = 0, \quad C_{nk} = nk\frac{\pi^2}{8L^2},$$

$$\Lambda^{(0)}_{ij} = \begin{cases} 2 & i=j=0 \\ \delta_{ij} & \text{otherwise} \end{cases}, \quad \delta_{ij} = \begin{cases} 1, & i=j, \\ 0, & i\neq j, \end{cases} \quad \Lambda^{(1)}_{nkj} = \Lambda^{(0)}_{|n-k|j} + \Lambda^{(0)}_{|n+k|j}, \quad \Lambda^{(2)}_{nkjp} = \Lambda^{(1)}_{|n-k|jp} + \Lambda^{(1)}_{|n+k|jp},$$
$$\Lambda^{(3)}_{nkjpq} = \Lambda^{(2)}_{|n-k|jpq} + \Lambda^{(2)}_{|n+k|jpq},$$

$$\Lambda^{(4)}_{nkjpqi} = \Lambda^{(3)}_{|n-k|jpqi} + \Lambda^{(3)}_{|n+k|jpqi}, \quad \Lambda^{(-1)}_{nkj} = \Lambda^{(0)}_{|n-k|j} - \Lambda^{(0)}_{|n+k|j}, \quad \Lambda^{(-2)}_{nkjp} = \Lambda^{(1)}_{|n-k|jp} - \Lambda^{(1)}_{|n+k|jp}, \quad \Lambda^{(-3)}_{nkjpq} = \Lambda^{(2)}_{|n-k|jpq} - \Lambda^{(2)}_{|n+k|jpq},$$
$$\Lambda^{(-4)}_{nkjpqi} = \Lambda^{(3)}_{|n-k|jpqi} - \Lambda^{(3)}_{|n+k|jpqi},$$

$$\Pi^{(1)}_{nki} = 4C_{nk}\Lambda^{(-1)}_{nki} + 2E_nE_k\Lambda^{(1)}_{nki}, \quad \Pi^{(2)}_{nkij} = 2C_{nk}(E_n+E_k)\Lambda^{(-2)}_{nkij} + 2(C_{nn}E_k + C_{kk}E_n)\Lambda^{(2)}_{nkij},$$

$$\Pi^{(3)}_{nkijp} = \tfrac{2}{3}\Big[2C_{nk}(C_{nn}+C_{kk}+E_nE_k)\Lambda^{(-3)}_{nkijp} + (E_nE_k(C_{nn}+C_{kk})+4C^2_{nk})\Lambda^{(3)}_{nkijp}\Big],$$

$$\Pi^{(4)}_{nkijpq} = \tfrac{1}{3}\Big[C_{nk}(E_n(C_{nn}+3C_{kk})+E_k(C_{kk}+3C_{nn}))\Lambda^{(-4)}_{nkijpq} + (E_nC_{nn}(C_{nn}+3C_{kk})+E_nC_{kk}(C_{kk}+3C_{nn}))\Lambda^{(4)}_{nkijpq}\Big],$$

$$V^{2,n}_{ab} = \tfrac{1}{2}\Lambda^{(1)}_{nab} - (4E_nE_a)^{-1}\Pi^{(1)}_{nab}, \quad V^{3,n}_{abc} = (2E_n)^{-1}C_{nn}\Lambda^{(2)}_{nabc} - (4E_nE_a)^{-1}\Pi^{(2)}_{nabc} - (2E_n)^{-1}V^{2,k}_{ab}\Pi^{(1)}_{nkc},$$

$$V^{4,n}_{abcd} = \tfrac{1}{6}C_{nn}\Lambda^{(3)}_{nabcd} - (4E_nE_a)^{-1}\Pi^{(3)}_{nabcd} - (2E_n)^{-1}V^{2,k}_{ab}\Pi^{(2)}_{nkcd} - (2E_n)^{-1}V^{3,k}_{abc}\Pi^{(1)}_{nkd},$$

$$V^{5,n}_{abcdf} = \tfrac{1}{2}E^{-1}_n C^2_{nn}\Lambda^{(4)}_{nabcdf} - (4E_nE_a)^{-1}\Pi^{(4)}_{nabcdf} - (2E_n)^{-1}V^{2,k}_{ab}\Pi^{(3)}_{nkcdf} - (2E_n)^{-1}V^{3,k}_{abc}\Pi^{(2)}_{nkdf} - (2E_n)^{-1}V^{4,k}_{abcd}\Pi^{(1)}_{nkf},$$

$$\overline{V}^{3,k}_{ijp} = \tfrac{1}{2}(V^{3,k}_{ijp}+V^{3,k}_{ipj}), \quad \overline{V}^{4,k}_{ijpq} = \tfrac{1}{3}(V^{4,k}_{ijpq}+V^{4,k}_{ipjq}+V^{4,k}_{iqpj}), \quad \overline{V}^{5,k}_{ijpqr} = \tfrac{1}{4}(V^{5,k}_{ijpqr}+V^{5,k}_{ipjqr}+V^{5,k}_{iqpjr}+V^{5,k}_{irpqj}),$$

$$d^{1,m}_{ab} = 2E_m(\tfrac{1}{2}\Lambda^{(1)}_{abm}+V^{2,m}_{ab}), \quad d^{2,m}_{abc} = 2E_m((2E_a)^{-1}C_{aa}\Lambda^{(2)}_{abcm}+E_n\Lambda^{(1)}_{ncm}V^{2,n}_{ab}+V^{3,m}_{abc}),$$

$$d^{3,m}_{abcd} = 2E_m(\tfrac{1}{6}C_{aa}\Lambda^{(3)}_{abcdm}+C_{nn}\Lambda^{(2)}_{ncdm}V^{2,n}_{ab}+E_n\Lambda^{(1)}_{ndm}V^{3,m}_{abc}+V^{4,m}_{abcd}),$$

$$d^{4,m}_{abcdf} = 2E_m(\tfrac{1}{12}C^2_{aa}E^{-1}_a\Lambda^{(4)}_{abcdfm}+\tfrac{1}{3}C_{nn}E_n\Lambda^{(3)}_{ncdfm}V^{2,n}_{ab}+C_{nn}\Lambda^{(2)}_{ndfm}V^{3,n}_{abc}+E_n\Lambda^{(1)}_{nfm}V^{4,m}_{abcd}+V^{5,m}_{abcdf}),$$

$$t^{0,m}_{ab} = 2E_m(V^{2,m}_{ab}+(8E_aE_b)^{-1}\Pi^{(1)}_{abm}), \quad t^{1,m}_{abc} = 2E_m(2\overline{V}^{3,m}_{abc}+V^{2,n}_{ab}E_n\Lambda^{(1)}_{ncm}+(4E_aE_b)^{-1}\Pi^{(2)}_{abmc}+(2E_a)^{-1}V^{2,n}_{bc}\Pi^{(1)}_{anm}),$$

$$t^{2,m}_{abcd} = 2E_m\Big(3\overline{V}^{4,m}_{abcd}+2\overline{V}^{3,n}_{abc}E_n\Lambda^{(1)}_{ndm}+V^{2,n}_{ab}C_{nn}\Lambda^{(2)}_{ncdm}+\tfrac{3}{8}\Pi^{(3)}_{abcdm}(E_aE_b)^{-1}+\Pi^{(2)}_{bncm}E^{-1}_bV^{2,n}_{ad}+(2E_b)^{-1}V^{3,n}_{acd}\Pi^{(1)}_{bnm} + \tfrac{1}{2}\Pi^{(1)}_{nkm}V^{2,k}_{ac}V^{2,n}_{bd}\Big),$$

$$t^{3,m}_{abcdf} = 2E_m\Big(4\overline{V}^{5,m}_{abcdf}+3\overline{V}^{4,m}_{abcd}E_n\Lambda^{(1)}_{nfm}+2\overline{V}^{3,n}_{abc}C_{nn}\Lambda^{(2)}_{ndfm}+\frac{1}{3}V^{2,n}_{ab}C_{nn}E_n\Lambda^{(3)}_{ncdfm}+\frac{1}{2}\Pi^{(4)}_{abmcdf}(E_aE_b)^{-1} + \frac{3}{2}\Pi^{(3)}_{nacdm}E^{-1}_aV^{2,n}_{bf}+\Pi^{(2)}_{nafm}E^{-1}_aV^{3,n}_{bcd}+\Pi^{(2)}_{nkfm}V^{2,k}_{ac}V^{2,n}_{bd}+\Pi^{(1)}_{anm}(2E_a)^{-1}V^{4,n}_{bcdf}+\Pi^{(1)}_{nkm}V^{3,k}_{acd}V^{2,k}_{bf}\Big),$$

$$D^m_1(a,b) = d^{1,m}_{ab}, \quad D^m_2(a,b,c) = \begin{cases} d^{2,m}_{abb}, & b=c, \\ d^{2,m}_{abc}+d^{2,m}_{acb}, & b\neq c, \end{cases}$$

$$D^m_3(a,b,c,d) = \begin{cases} d^{3,m}_{abbb}, & b=c=d, \\ d^{3,m}_{abbd}+d^{3,m}_{abdb}+d^{3,m}_{adbb}, & b=c, c\neq d, \\ d^{3,m}_{abcc}+d^{3,m}_{acbc}+d^{3,m}_{accb}, & b\neq c, c=d, \\ d^{3,m}_{abcd}+d^{3,m}_{abdc}+d^{3,m}_{acbd}+d^{3,m}_{acdb}+d^{3,m}_{adbc}+d^{3,m}_{adcb}, & b\neq c, c\neq d, \end{cases}$$

$$D_4^m(a,b,c,d,f)=\begin{cases} d_{abbbb}^{4,m}, & b=c=d=f,\\ d_{abbbf}^{4,m}+d_{abbfb}^{4,m}+d_{abfbb}^{4,m}+d_{afbbb}^{4,m}, & b=c=d,d\neq f,\\ d_{accbc}^{4,m}+d_{acccb}^{4,m}+d_{abccc}^{4,m}+d_{acbcc}^{4,m}, & b\neq c,c=d=f,\\ d_{accdd}^{4,m}+d_{addcc}^{4,m}+d_{acdcd}^{4,m}+d_{adcdc}^{4,m}+d_{acddc}^{4,m}+d_{adccd}^{4,m}, & b=c,c\neq d,d=f,\\ d_{abbdf}^{4,m}+d_{abbfd}^{4,m}+d_{abdfb}^{4,m}+d_{abfdb}^{4,m}+d_{adfbb}^{4,m}+d_{afdbb}^{4,m}\\ +d_{afbbd}^{4,m}+d_{adbbf}^{4,m}+d_{abdbf}^{4,m}+d_{abfbd}^{4,m}+d_{afbdb}^{4,m}+d_{adbfb}^{4,m}, & b=c,c\neq d,d\neq f,\\ d_{accbf}^{4,m}+d_{accfb}^{4,m}+d_{acbfc}^{4,m}+d_{acfbc}^{4,m}+d_{abfcc}^{4,m}+d_{afbcc}^{4,m}\\ +d_{afccb}^{4,m}+d_{abccf}^{4,m}+d_{acbcf}^{4,m}+d_{acfcb}^{4,m}+d_{afcbc}^{4,m}+d_{abcfc}^{4,m}, & b\neq c,c=d,d\neq f,\\ d_{affbc}^{4,m}+d_{affcb}^{4,m}+d_{afbcf}^{4,m}+d_{afcbf}^{4,m}+d_{abcff}^{4,m}+d_{acbff}^{4,m}\\ +d_{abffc}^{4,m}+d_{acffb}^{4,m}+d_{afcfb}^{4,m}+d_{afbfc}^{4,m}+d_{abfcf}^{4,m}+d_{acfbf}^{4,m}, & b\neq c,c\neq d,d=f,\\ d_{abcdf}^{4,m}+d_{acdfb}^{4,m}+d_{abcfd}^{4,m}+d_{acbfd}^{4,m}+d_{abdfc}^{4,m}+d_{acdfb}^{4,m}\\ +d_{abfdc}^{4,m}+d_{acfdb}^{4,m}+d_{adfcb}^{4,m}+d_{afdcb}^{4,m}+d_{adfbc}^{4,m}+d_{afdbc}^{4,m}\\ +d_{abdcf}^{4,m}+d_{acdbf}^{4,m}+d_{abfcd}^{4,m}+d_{acfbd}^{4,m}+d_{adcfb}^{4,m}+d_{afbdc}^{4,m}\\ +d_{adbfc}^{4,m}+d_{afbdc}^{4,m}+d_{adbcf}^{4,m}+d_{afcbd}^{4,m}+d_{adcbf}^{4,m}+d_{afcbd}^{4,m}, & b\neq c,c\neq d,d\neq f, \end{cases}$$

$$T_0^m(a,b)=\begin{cases} t_{aa}^{0,m}, & a=b\\ t_{ab}^{0,m}+t_{ba}^{0,m}, & a\neq b \end{cases},\quad T_1^m(a,b,c)=\begin{cases} t_{aac}^{1,m}, & a=b\\ t_{abc}^{1,m}+t_{bac}^{1,m}, & a\neq b \end{cases},$$

$$T_2^m(a,b,c,d)=\begin{cases} t_{aacc}^{2,m}, & a=b,c=d\\ t_{abcc}^{2,m}+t_{bacc}^{2,m}, & a\neq b,c=d\\ t_{aacd}^{2,m}+t_{aadc}^{2,m}, & a=b,c\neq d\\ t_{abcd}^{2,m}+t_{bacd}^{2,m}+t_{abdc}^{2,m}+t_{badc}^{2,m}, & a\neq b,c\neq d \end{cases},$$

$$T_3^m(a,b,c,d,f)=\begin{cases} t_{aaccc}^{3,m} & a=b,c=d=f\\ t_{aaccf}^{3,m}+t_{aacfc}^{3,m}+t_{aafcc}^{3,m} & a=b,c=d,d\neq f\\ t_{aacdd}^{3,m}+t_{aadcd}^{3,m}+t_{aaddc}^{3,m} & a=b,c\neq d,d=f\\ t_{aacdf}^{3,m}+t_{aacfd}^{3,m}+t_{aadcf}^{3,m}+t_{aadfc}^{3,m}+t_{aafcd}^{3,m}+t_{aafdc}^{3,m} & a=b,c\neq d,d\neq f\\ t_{abccc}^{3,m}+t_{baccc}^{3,m} & a\neq b,c=d=f\\ t_{abccf}^{3,m}+t_{abcfc}^{3,m}+t_{baccf}^{3,m}+t_{bacfc}^{3,m}+t_{abfcc}^{3,m}+t_{bafcc}^{3,m} & a\neq b,c=d,d\neq f\\ t_{abcdd}^{3,m}+t_{abdcd}^{3,m}+t_{bacdd}^{3,m}+t_{badcd}^{3,m}+t_{abddc}^{3,m}+t_{baddc}^{3,m} & a\neq b,c\neq d,d=f\\ t_{abcdf}^{3,m}+t_{abcfd}^{3,m}+t_{bacdf}^{3,m}+t_{bacfd}^{3,m}+t_{abdcf}^{3,m}+t_{badcf}^{3,m}\\ +t_{abdfc}^{3,m}+t_{badfc}^{3,m}+t_{abfcd}^{3,m}+t_{abfdc}^{3,m}+t_{bafcd}^{3,m}+t_{bafdc}^{3,m} & a\neq b,c\neq d,d\neq f \end{cases},$$

References

Bateman, H., 1944. Partial Differential Equations of Mathematical Physics. Dover.

Faltinsen, O.M., Rognebakke, O.F., Lukovsky, I.A., Timokha, A.N., 2000. Multidimensional modal analysis of nonlinear sloshing in a rectangular tank with finite water depth. Journal of Fluid Mechanics 407, 201–234.

Faltinsen, O.M., Timokha, A.N., 2001. An adaptive multimodal approach to nonlinear sloshing in a rectangular tank. Journal of Fluid Mechanics 432, 167–200.

Faltinsen, O.M., Rognebakke, O.F., Timokha, A.N., 2005. Classification of three-dimensional nonlinear sloshing in a square-base tank with finite depth. Journal of Fluids and Structures 20, 81–103.

Hargreaves, R., 1908. A pressure-integral as kinetic potential. Philosophical Magazine (6) 16 (no. 3), 436–444.

Kaneko, S., Yoshida, O., 1999. Modeling of deepwater-type rectangular tuned liquid damper with submerged nets. ASME Journal of Pressure Vessel Technology 121, 413–422.

Kareem, A., Kiljewski, T., Tamura, Y., 1999. Mitigation of motions of tall buildings with specific examples of recent applications. Wind and Structures 2, 201–251.

Le Mehaute, B., 1976. An Introduction to Hydrodynamics and Water Waves. Springer-Verlag, New York.

Lepellitier, T.G., Raichlen, F., 1988. Nonlinear oscillations in rectangular tanks. Journal of Engineering Mechanics 114 (1), 1–23.

Luke, J.C., 1967. A variational principle for a fluid with a free surface. Journal of Fluid Mechanics 27, 297–395.

Miles, J.W., 1967. Surface wave damping in closed basins. Proceedings of the Royal Society of London 297, 459–475.

Morison, J.R., O'Brien, M.P., Johnson, J.W., Schaaf, S.A., 1950. The forces exerted by surface waves on piles. AIME Petroleum Transactions 189, 149–154.

Tadjbakhsh, I., Keller, J.B., 1960. Standing surface waves of finite amplitude. Journal of Fluid Mechanics 8, 442–451.

Tait, M.J., 2004. The performance of 1-D and 2-D tuned liquid dampers. Ph.D. Dissertation, The University of Western Ontario, London, Ontario, Canada.

Tait, M.J., 2008. Modelling and preliminary design of a structure–TLD system. Engineering Structures 30, 2644–2655.

Tait, M.J., El Damatty, A.A., Isyumov, N., Siddique, M.R., 2005. Numerical flow model to simulate tuned liquid dampers (TLD) with slat screens. Journal of Fluids and Structures 20, 1007–1023.

Vickery, B.J., Davenport, A.G., 1970. An investigation of the behaviour in wind of the proposed centrepoint tower. Research Report BLWT-1-70, Sydney, Australia.

Warburton, G.B., 1982. Optimum absorber parameters for various combinations of response and excitation parameters. Earthquake Engineering and Structural Dynamics 10, 381–401.

Waterhouse, D.D., 1994. Resonant sloshing near a critical depth. Journal of Fluid Mechanics 281, 313–318.